Science of the Total Environment 584–585 (2017) 105–117

Contents lists available at ScienceDirect

Science of the Total Environment

journal homepage: www.elsevier.com/locate/scitotenv

Source apportionment of ambient fine and coarse particulate matter at the Fort McKay community site, in the Athabasca Oil Sands Region, Alberta, Canada

Matthew S. Landis [a,*], J. Patrick Pancras [b], Joseph R. Graney [c], Emily M. White [d], Eric S. Edgerton [e], Allan Legge [f], Kevin E. Percy [g]

[a] Integrated Atmospheric Solutions, LLC., Cary, NC, USA
[b] Pancras Consulting, Cary, NC, USA
[c] Geological Sciences and Environmental Studies, Binghamton University, Binghamton, NY, USA
[d] Maed Consulting, Chapel Hill, NC, USA
[e] Atmospheric Research & Analysis, Inc., Cary, NC, USA
[f] Biosphere Solutions, Calgary, Alberta, Canada
[g] Air Quality Effects Consulting Ltd., Fredericton, New Brunswick, Canada

HIGHLIGHTS

- Fine and coarse particulate matter was quantified in Fort McKay, Alberta.
- Receptor modeling elucidated and quantified significant contributing sources.
- 58% of $PM_{2.5}$ and 83% of $PM_{10-2.5}$ was attributable to oil sands production operations.
- 25% of the observed $PM_{2.5}$ was attributed to biomass combustion.

GRAPHICAL ABSTRACT

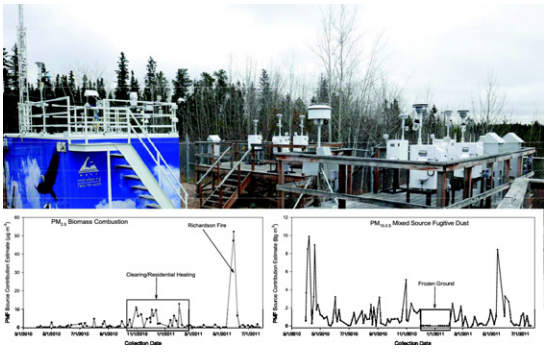

ARTICLE INFO

Article history:
Received 16 December 2016
Received in revised form 16 January 2017
Accepted 16 January 2017
Available online 29 January 2017

Editor: D. Barcelo

Keywords:
Fugitive dust
Positive matrix factorization
Wildland fire
Smoke
Fine and coarse particulate matter

ABSTRACT

An ambient air particulate matter sampling study was conducted at the Wood Buffalo Environmental Association (WBEA) AMS-1 Fort McKay monitoring station in the Athabasca Oil Sand Region (AOSR) in Alberta, Canada from February 2010 to July 2011. Daily 24 h integrated fine ($PM_{2.5}$) and coarse ($PM_{10-2.5}$) particulate matter was collected using a sequential dichotomous sampler. Over the duration of the study, 392 valid daily dichotomous $PM_{2.5}$ and $PM_{10-2.5}$ sample pairs were collected with concentrations of $6.8 \pm 12.9\ \mu g\ m^{-3}$ (mean ± standard deviation) and $6.9 \pm 5.9\ \mu g\ m^{-3}$, respectively. A subset of 100 filter pairs was selected for element analysis by energy dispersive X-ray fluorescence and dynamic reaction cell inductively coupled plasma mass spectrometry. Application of the U.S. EPA positive matrix factorization (PMF) receptor model to the study data matrix resolved five $PM_{2.5}$ sources explaining 96% of the mass including oil sands upgrading (32%), fugitive dust (26%), biomass combustion (25%), long-range Asian transport lead source (9%), and winter road salt (4%). An analysis of historical $PM_{2.5}$ data at this site shows that the impact of smoke from wildland fires was particularly high during the summer of 2011. PMF resolved six $PM_{10-2.5}$ sources explaining 99% of the mass including fugitive haul road dust (40%), fugitive oil sand (27%), a mixed source fugitive dust (16%), biomass combustion (12%), mobile source (3%), and a local

* Corresponding author.
E-mail address: mlandis@atmospheric-solutions.com (M.S. Landis).

http://dx.doi.org/10.1016/j.scitotenv.2017.01.110

copper factor (1%). Results support the conclusion of a previous epiphytic lichen biomonitor study that near-field atmospheric deposition in the AOSR is dominated by coarse fraction fugitive dust from bitumen mining and upgrading operations, and suggest that fugitive dust abatement strategies targeting the three major sources of $PM_{10-2.5}$ (e.g., oil sand mining, haul roads, bulk material stockpiles) would significantly reduce near-field atmospheric deposition gradients in the AOSR and reduce ambient PM concentrations in the Fort McKay community.

1. Introduction

The Athabasca Oil Sands Region (AOSR) in northern Alberta, Canada contains economically recoverable petroleum reserves estimated to be approximately 170 billion barrels (Attanasi and Meyer, 2010; Alberta Energy, 2017). These proven petroleum reserves rank the AOSR third in the world behind Saudi Arabia and Venezuela. Oil production in the AOSR has been steadily increasing over the last decade from 0.6 million barrels per day in 2000, to 2.3 million barrels per day in 2014 (Alberta Energy, 2017). Synthetic crude oil production from bitumen in the AOSR is accomplished using a combination of surface mining and drilling (in situ) production. Of the proven reserves, it is estimated that 20% of the bitumen will ultimately be recovered through surface mining and 80% from in-situ production techniques (Government of Alberta, 2008). The type and magnitude of inorganic air pollutants emitted from these two extraction techniques are unique compared to other air emission sources. Quantifying their relative contribution to observed ambient particulate matter (PM) concentrations and atmospheric deposition are critical to emission mitigation and local environmental impact management. A lichen biomonitoring study identified the fugitive emission of coarse mode PM ($PM_{10-2.5}$) from oil sand production activities as the primary driver of the observed atmospheric deposition and spatial patterns in the AOSR (Landis et al., 2012).

Surface mining in the AOSR results in large-scale land disturbance similar to coal, copper, gold, and other traditional mining operations. Currently, the soil and glacial till overlaying the oil sand deposits (over burden) is removed and the exposed oil sands are excavated and transported for processing using large scale shovel and truck hauling operations. Atmospheric pollution from shovel and truck fleet operations mainly consists of fugitive PM emissions (wind-blown dust) and diesel engine combustion exhaust (Landis et al., 2012; Wang et al., 2015; Wang et al., 2016). Bitumen is separated from the sand and clay matrix components of the oil sands using a warm water frothing technique (Masliyah et al., 2004; Osacky et al., 2013), and in four of the current commercial operations is upgraded to sweet light synthetic crude on site. Upgrading by-products, such as elemental sulfur and petroleum coke, are in many cases consolidated in large on-site storage piles (Zhang et al., 2016). The water, sand, and clay waste streams are pumped to large tailings ponds where much of the water is recycled; the sand and clay are consolidated and used for mine reclamation activities. Limestone in the AOSR is quarried, crushed, and used for development of haul roads and other construction activities. Overburden stored for future mine reclamation, haul roads, petroleum coke storage piles, tailings ponds, and limestone quarrying and crushing operations are all potential sources of fugitive wind-blown dust (Landis et al., 2012; Zhang et al., 2016).

This paper presents results from a study designed to quantify the ambient $PM_{2.5}$ (fine) and $PM_{10-2.5}$ (coarse) concentrations, and identify the contributions from emission sources to Fort McKay, a centrally located First Nation and Metis community, in the AOSR previously identified as being impacted by emissions from nearby oil sand bitumen production operations (Landis et al., 2012). $PM_{2.5}$ concentration trends measured at the site from 1999 to 2015 are presented to place the current measurements into historic context, and a seasonal analysis of source apportionment results highlights the importance of temporal monitoring representativeness.

2. Methods

2.1. Sampling site

The Wood Buffalo Environmental Association (WBEA) AMS-1 Bertha Ganter-Fort McKay ambient air monitoring station (57°11′21.70″ N; −111°38′26.06″ W) is located in the Fort McKay First Nation and Metis community. This monitoring site was originally established in 1983 as an Alberta Environment Station, and was subsequently incorporated into the WBEA network, moved to its current location, and upgraded in 1997. AMS-1 currently provides real-time ambient air quality information including the Air Quality Health Index (AQHI) to the community. The AMS-1 site is located in an area that is in close proximity to ongoing oil sand production operations such as mining, separating, and upgrading of bitumen (Fig. 1). Routine WBEA ambient monitoring data including continuous (i) $PM_{2.5}$ mass measured using ThermoScientific (Franklin, MA) Model 1400B Tapered Element Oscillating Microbalance (TEOM) from 1998 to June 2011 and a ThermoScientific Model 5030 Synchronized Hybrid Ambient Real-time Particulate Monitor (SHARP) from June 2011 to present, (ii) total oxides of nitrogen (NO_x) measured using a ThermoScientific Model 42i chemiluminescence analyzer, (iii) sulfur dioxide (SO_2) measured using a ThermoScientific Model 43i pulsed fluorescence analyzer, and (iv) ammonia (NH_3) measured using a ThermoScientific Model 17i chemiluminescence analyzer (WBEA, 2011) were incorporated into this study.

2.2. Collection and weighing of filter-based ambient particulate matter samples

Twenty-four hour ambient PM samples for mass, sulfur, and element determination were collected on a daily basis onto Teflon filters using a ThermoScientific Model 2025D Sequential Dichotomous air sampler (a U.S. EPA designated Federal Equivalent Method for $PM_{2.5}$) from February 22, 2010 through July 27, 2011. The dichotomous sampler utilized a PM_{10} impactor inlet operating at 16.7 LPM to make the initial particle size cutoff at 10 μm mass median aerodynamic diameter (MMAD). The virtual impactor or "dichotomous splitter," followed the PM_{10} impactor inlet and dynamically segregated the particles into fine (≤2.5 μm) and coarse (10–2.5 μm) size fractions that were collected onto two separate filters (Loo and Cork, 1988). The virtual impactor accelerated incoming PM_{10} aerosols using a jet to impart sufficient momentum that they resisted the lateral sheer of the major flow and traversed into the receiving jet and were captured onto the coarse filter. Calibrated mass flow controllers maintained the fine particle filter flow at 15.0 LPM and the coarse particle filter flow at 1.67 LPM to ensure the correct MMAD size cut.

The virtual impactor resulted in the collection of all coarse mode particles from the total flow (16.7 L min^{-1}) plus the fine mode particles in the minor flow (1.67 L min^{-1}) on the coarse filter. As a result, the fine mode and corrected coarse mode concentrations (mass, sulfur, and elements) are adjusted for this artifact using Eqs. (1) and (2), respectively.

$$C_{Fine} = \left(\frac{M_{Fine}}{V_{Fine}}\right) \quad (1)$$

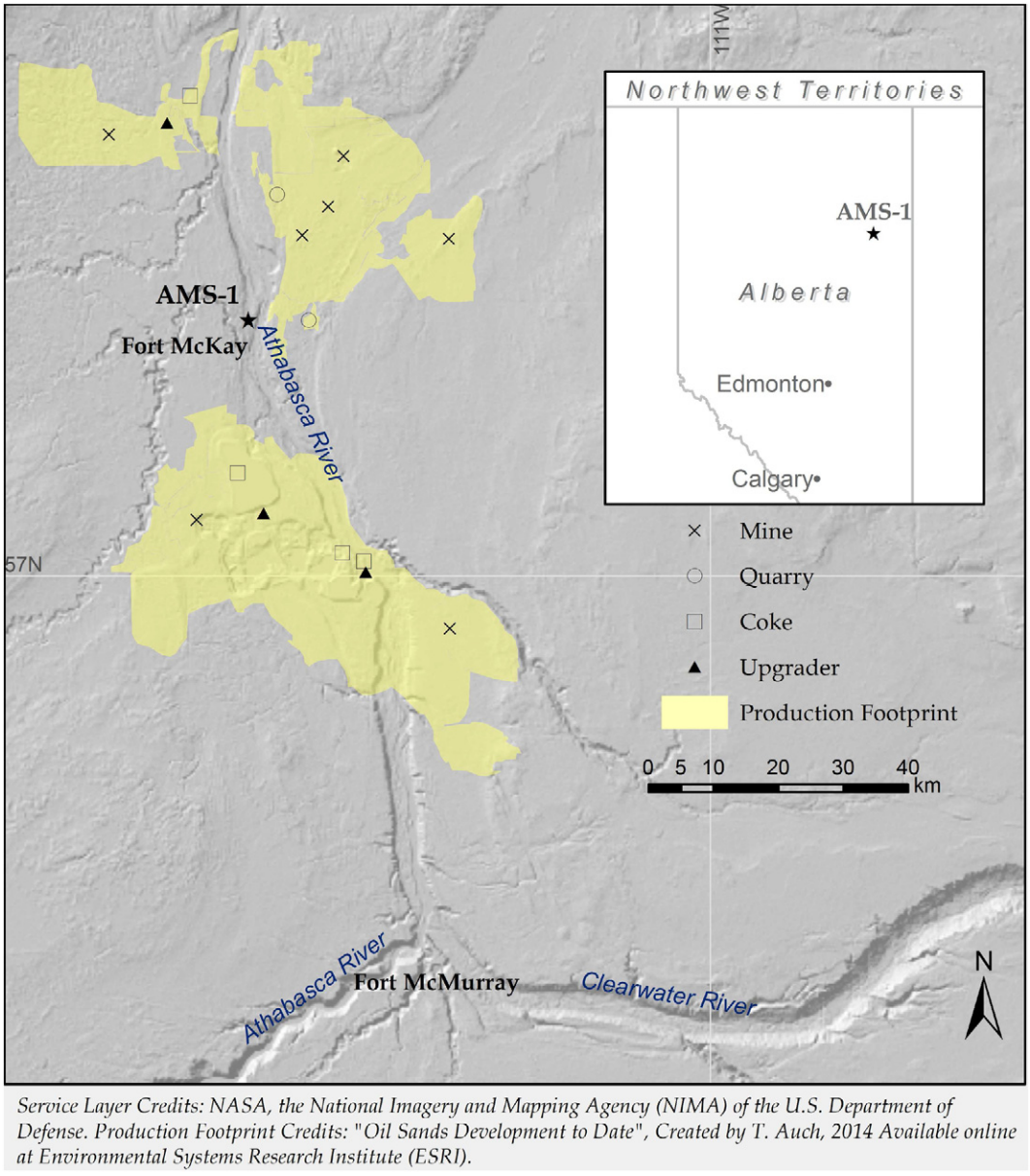

Fig. 1. Map depicting the location of the WBEA AMS-1 Fort McKay ambient monitoring station and the surrounding major oil sand bitumen production facilities operating during the 2010–2011 study time period.

$$C_{Coarse} = \left[\frac{M_{Coarse} - \left(\frac{M_{Fine} * V_{Coarse}}{V_{Fine}}\right)}{V_{Total}}\right] \quad (2)$$

where:

C_{Fine} = concentration $PM_{2.5}$ (μg m^{-3})
C_{Coarse} = concentration PM_{Coarse} (μg m^{-3})
V_{Fine} = volume of air through $PM_{2.5}$ filter (m^3)
V_{Coarse} = volume of air through PM_{Coarse} filter (m^3)
V_{Total} = volume of air through sampler (m^3)
M_{Fine} = mass on fine filter (μg)
M_{Coarse} = mass on coarse filter (μg)

Measurement Technologies Laboratories (MTL; Minneapolis, MN) 47 mm Teflon membrane filters with Teflon support rings were procured, pre-weighed, installed into individual filter cassettes and then into multi-cassette magazines, shipped to WBEA, received back from WBEA, and post-weighed by Atmospheric Research & Analysis, Inc. (ARA, Morrisville, NC). Each filter magazine was loaded with enough filter cassettes for two weeks of unattended sampling and a field blank. The standard ThermoScientific stainless steel filter support screens were replaced with custom cross-linked Teflon-coated support screens in the filter cassettes to avoid potential trace level metals contamination of the filters. Filters were pre- and post-weighed in a Class 1000 clean environment using a Mettler Toledo (Columbus, OH) Model UMX2 microbalance fitted with an MTL Model AH225-6 robotic auto-handler. The ARA clean environment maintains temperature (±0.1 °C) and relative humidity (±2%) within strict tolerances to ensure consistent results. The MTL AH225 system performs five replicate weighings of each filter and automatically minimizes electrostatic effects by utilizing a static discharge Po α-particle emission and Faraday pan. The balance is zeroed before and after each filter weighing and one National Institute of Standards and Technology (NIST) traceable Class A weight and two unexposed reference filters are weighed every 6 h. 3-Sigma uncertainties for the NIST-traceable weight and reference filters are typically 1.0 microgram and 1.6 microgram, respectively, equivalent to <0.1 μg m^{-3} for a 24-hour sample. Zero and buoyancy corrections

were performed and the mean ± standard deviation weight of each filter was reported.

For this study, the dichotomous sampler was configured to run daily (24 h) integrated samples every day starting at 00:00 MST. The two sample filter magazines were installed and each filter ID number was entered into the dichotomous sampler's electronic interface for sample tracking and for logging instrument performance during each sample collection period. Each magazine arrived at the site with a sample tracking form for the entire magazine, where the sample ID and filter IDs were documented. Each magazine was sent with at least one field blank to be shuttled through the sampler. Data downloaded from the dichotomous sampler included sample ID, filter ID, sample duration, flows, sampled air volume, and any error codes for a comprehensive documentation of the ambient air samples. WBEA technicians routinely performed flow checks, leak checks, and time checks in the field. Flow checks employed a NIST traceable BGI-MESA Labs (Butler, NJ) DeltaCal primary flow standard.

2.3. X-ray fluorescence analysis

After being conditioned in the weighing chamber for a minimum of 24 h at 35% relative humidity (±5%) and 21 °C (±1 °C), all Teflon filters were post-weighed and analyzed for total sulfur using a PANalytical (Almelo, Netherlands) Model Epsilon 5 energy-dispersive X-ray fluorescence (ED-XRF) analyzer. ED-XRF is commonly used as a nondestructive analytical method for quantifying elemental content in ambient PM samples (Solomon et al., 2001). EDXRF involves excitation of the constituent atoms in a sample with a nearly bi-chromatic X-ray beam from a secondary target. As the atoms relax back to the ground state, they emit X-rays whose energies are characteristic of the element. The fluorescent X-rays impinge on a detector and the resulting spectrum has an energy profile that is directly related to the elements and their concentrations in the sample. The spectra are subsequently processed. Multiple linear regression analysis is used to de-convolute the pulse height spectrum into its background and constituent element peaks by least-squares fitting of stored elemental thin-film library spectra and lot specific MTL filter backgrounds. Subsequent processing performs attenuation and interference corrections and converts raw data to reportable information. Calibrations were performed empirically with MicroMatter (Surrey, BC) thin-film standards, and verified via analysis of U.S. NIST Standard Reference Material (SRM) #2783 (Air Particulate Matter on Filter Media).

2.4. Teflon filter extraction and trace element analysis

Following ED-XRF analysis, the dichotomous sampler filters were digested using a CEM Corporation (Matthews, NC) Mars Express microwave digestion system in a mixture of ultra-pure H_2O_2, HF and HNO_3 with heating to 180 °C for 40 min in a procedure similar to that developed by Jalkanen and Häsänen (1996). After cooling, American Society of Testing and Materials (ASTM) Type I ultrapure (18.2 MΩ·cm) water was added to each vessel to bring the extract up to a final volume of 15 ml. A 25–30 mg aliquot of NIST SRM 1633c was also digested with each batch of 30–35 filters.

The sample extracts were then analyzed for a suite of elements (Al, Sb, As, Ba, Be, Bi, Cd, Ca, Ce, Cs, Cr, Co, Cu, Fe, La, Pb, Li, Mg, Mn, Mo, Nd, Ni, Nb, P, Pt, K, Pr, Rb, Sa, Se, Si, Na, Sr, Ta, Tl, Th, Sn, Ti, W, U, V, Zn) using a Perkin-Elmer (Waltham, MA) Model 9000 Elan-II dynamic reaction cell inductively coupled plasma mass spectrometry (DRC-ICPMS). Clean handling techniques were used in all stages of the analysis to prevent contamination. Particle-free gloves were worn at all times and all labware with which the samples and reagents come into contact was acid cleaned. Just prior to analysis, an aliquot of the sample was transferred to a small polypropylene auto sampler vial. The samples were introduced into the DRC-ICPMS by pneumatic nebulization. Peak characteristics for each target element were considered in the method to eliminate interferences from polyatomic ions derived from the plasma gas, reagents, or sample matrix. Instrument drift and suppression, or enhancement of instrument response caused by the sample matrix, was corrected by internal standardization (Edgerton et al., 2012). Target isotopes and study specific MDLs are summarized in Appendix Table A.1.

2.5. Source apportionment modeling

According to Hopke (2009, 2016), source apportionment is the estimation of the contributions to the pollutant concentrations resulting from emissions from multiple natural and anthropogenic sources. Forensic data (mathematical and/or statistical) analysis tools called *receptor models* are applied to extract information on the sources of air pollutants from the measured constituent concentrations at a receptor

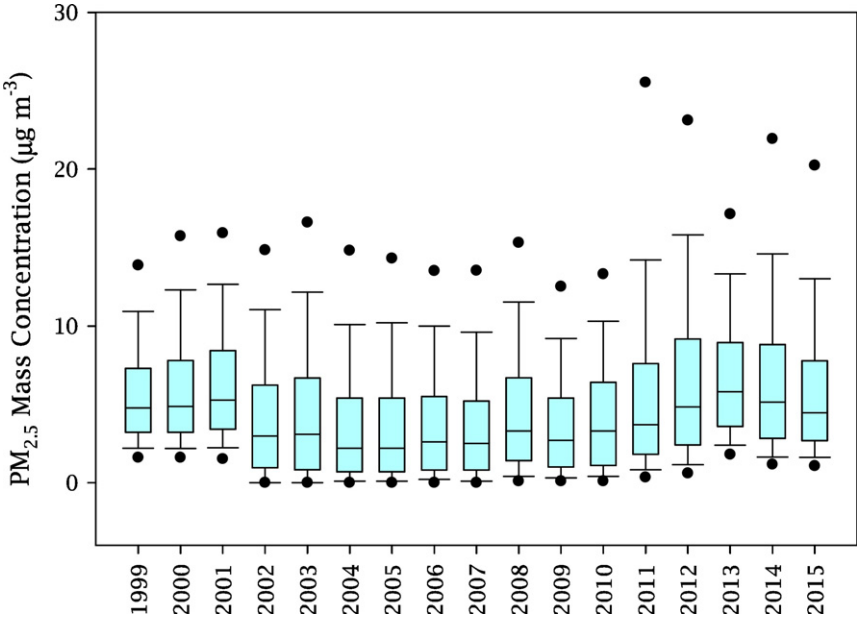

Fig. 2. Annual $PM_{2.5}$ mass distributions at Fort McKay (1999–2015).

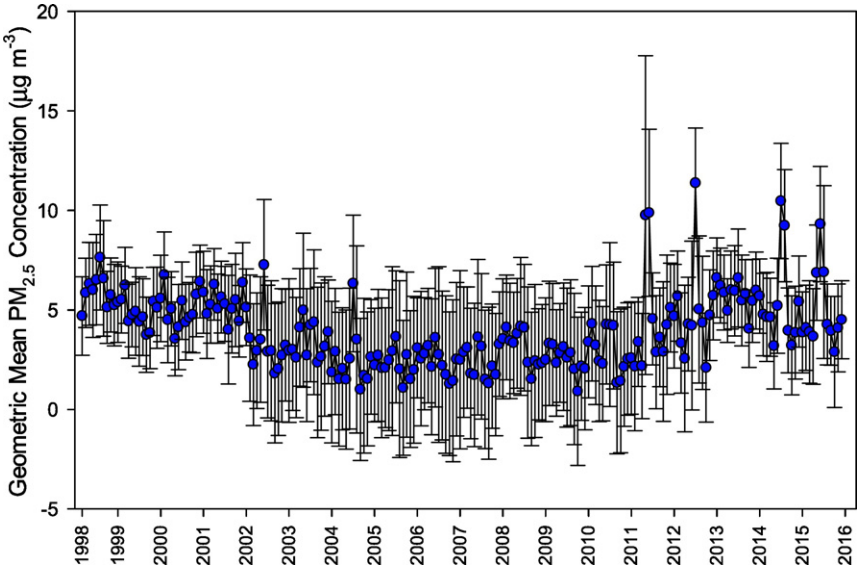

Fig. 3. Monthly geometric mean $PM_{2.5}$ concentrations at Fort McKay (1999–2015).

location. Unlike deterministic dispersion air quality models, receptor models generally do not use pollutant emissions, meteorological data, or chemical transformation mechanisms to estimate the contribution of sources to receptor concentrations. Instead, receptor models use mathematically detectable characteristics (chemical and physical) of gases and particles measured at a monitoring or receptor site to both identify and quantify source contributions to receptor concentrations. The multivariate EPA Positive Matrix Factorization (PMF) v4.2 receptor model (U.S. EPA, 2011) was used for this study. Briefly, the EPA implementation of PMF uses a graphical user interface that has been developed on the PMF model, and the general mixed linear model is solved using the Multilinear Engine-2 (ME-2) program (Paatero, 1999). EPA PMF operates in a robust mode, meaning outlier species concentrations are not allowed to overly influence the factor solutions. Additionally, the feature of individual weighting of each data point allows the model to calculate covariance in the receptor data matrix on the basis of reliability of the chemical measurements. Block bootstrapping (BBS) was used to estimate variability in the source contribution estimates (U.S. EPA, 2011). The block bootstrap method captures effects from random errors in the solution, and also partially accounts for errors from computational rotational ambiguity.

Atmospheric elemental concentrations that were at or below the method detection limit (MDL) concentrations were substituted with MDL/2 in the PMF input data files. Daily average concentrations of SO_2, NO_x, and NH_3 were calculated from 5-min WBEA AMS-1 site ambient monitoring data for PMF modeling purposes, and combined with the dichotomous sampler particulate matter dataset. Point-wise uncertainty for PMF analysis was estimated using MDL and the DRC-ICPMS analysis precision (one sigma from replicate measurements) values by using Eq. (3).

$$uncertainty = \sqrt{(\mathrm{MDL})^2 + (analysis\ precision)^2} \quad (3)$$

Uncertainties for values below MDL values were calculated as 5/6 * MDL, and for missing values as 4 * median concentrations (Pancras et al., 2013).

3. Results and discussion

3.1. Fort McKay historical ambient $PM_{2.5}$

The long-term $PM_{2.5}$ trend at the AMS-1 Fort McKay monitoring site was evaluated to place the results from this study's particulate matter monitoring into a historical perspective. The bar (25th–75th percentile) and whisker (10th–90th percentile) plot presented in Fig. 2 depicts the annualized distribution of hourly observations. The median long-term $PM_{2.5}$ concentration record does not indicate a significant trend, however four out of the last five years have elevated wildland fire smoke impacted concentration outliers signified as 95th percentile dots (e.g.,

Table 1
Summary of AMS-1 ambient measurements (February 22, 2010–July 25, 2011).

Analyte	n	Units	Mean	Std. Dev.	Min	Q1	Median	Q3	Max
$PM_{2.5}$ mass (Dichot)	392	µg m^{-3}	6.8	12.9	0.1	3.1	4.7	7.1	170.5
$PM_{10-2.5}$ mass (Dichot)	392	µg m^{-3}	6.9	5.9	0.1	2.4	5.2	9.5	30.2
$PM_{2.5}$ mass (Dichot)	100	µg m^{-3}	8.6	21.6	0.5	3.7	5.0	7.0	170.5
$PM_{10-2.5}$ mass (Dichot)	100	µg m^{-3}	7.6	5.9	0.5	3.2	6.7	10.6	26.3
$PM_{2.5}$ mass (TEOM)[a]	10864	µg m^{-3}	8.5	30.2	0.1	1.4	3.4	6.8	449.8
Sulfur dioxide[a]	11308	ppb	1.5	3.8	0.0	0.2	0.7	1.3	82.7
Oxides of nitrogen[a]	11339	ppb	10.0	14.4	0.0	1.2	4.7	12.4	193.0
Ammonia[a]	11193	ppb	0.4	13.5	0.0	0.0	0.0	0.0	122.9

Note: Shaded dichotomous samples selected for ED-XRF and DRC-ICPMS element analysis.
[a]Hourly integrated continuous measurements.

Table 2
Summary statistics of invalid AMS-1 samples from May 18–June 15, 2011 during wildland fire event impacts.

	n	Units	Mean	Std. Dev.	Min	Q1	Median	Q3	Max
$PM_{2.5}$	7	μg m^{-3}	351.7	157.3	152.0	175.9	423.8	479.5	522.9
$PM_{10-2.5}$	7	μg m^{-3}	44.3	11.0	36.9	38.5	40.4	44.5	68.5

2011, 2012, 2014 and 2015) in Fig. 2. The impact of the statistical outliers is highlighted in a time series analysis of the annual mean $PM_{2.5}$ mass concentration trend from 1999 to 2015, which was found to be significantly increasing ($p = 0.040$). However, the annual median ($p = 0.438$), 75th percentile ($p = 0.192$), and the 90th percentile ($p = 0.071$) annual concentrations revealed no significant trend (Appendix Fig. B.1). The annual 95th percentile concentrations show a significant positive trend ($p = 0.019$), suggesting that a small number of very high concentration events are driving the trend in annual averages. For this reason, time series analysis of air pollution data is commonly evaluated using the geometric mean (WHO, 1980). The monthly geometric mean of hourly $PM_{2.5}$ concentrations at the AMS-1 Fort McKay monitoring site are presented in Fig. 3. The months with exceptional wildland fire smoke impacts are clearly observable in the summers of 2011, 2012, 2014, and 2015, however no significant overall $PM_{2.5}$ concentration trend was found ($p = 0.802$).

3.2. Fort McKay ambient dichotomous sampler monitoring results

Over the course of the study, 392 valid daily dichotomous $PM_{2.5}$ and $PM_{10-2.5}$ sample pairs were collected with concentrations of 6.8 ± 12.9 μg m^{-3} (mean ± standard deviation) and 6.9 ± 5.9 μg m^{-3}, respectively (Table 1). The impact of wildland fire smoke emissions on both $PM_{2.5}$ and $PM_{10-2.5}$ mass were apparent during this study period, consistent with an epiphytic lichen biomonitoring source apportionment study in the AOSR (Landis et al., 2012). Many past high concentration $PM_{2.5}$ concentration episodes in the AOSR have been anecdotally associated with wildland fires based on visible smoke and a characteristic odor. In this study, from May 18, 2011 through June 15, 2011, the dichotomous sampler at the AMS-1 site automatically shut down seven times due to the high filter loading associated with the Richardson Backcountry wildland fire smoke impact events (Appendix Fig. B.2). When the loading on the filter reaches a point where the flow was reduced to below 90% of the programmed set point of either channel, the dichotomous sampler shut off to (i) prevent damage to the system and (ii) to prevent the PM_{10} and $PM_{2.5}$ MMAD cut points from significantly deviating. When the sampler reached the start time for the next sample the filters were exchanged and the sampler started again until those filters were also overloaded. While samples that run <23 h are considered invalid and are not acceptable indicators of the daily concentrations, the concentrations are representative of that period of time when the

Table 3
Statistical summary of mass and trace elements in ambient $PM_{2.5}$.

Analyte	n	Isotope	Unit	Mean	Std. Dev.	Min	Q1	Median	Q3	Max
$PM_{2.5}$ mass	100	–	μg m^{-3}	8.59	21.59	0.48	3.72	4.97	6.98	170.46
Aluminum	100	27	ng m^{-3}	41.39	38.06	−2.74	10.51	34.45	58.39	177.39
Antimony	100	123	ng m^{-3}	0.069	0.152	0.000	0.014	0.031	0.065	1.298
Arsenic oxide	100	91	ng m^{-3}	0.106	0.107	0.002	0.040	0.073	0.132	0.626
Barium	100	137	ng m^{-3}	0.134	3.073	−2.068	−1.380	−0.269	0.651	25.845
Beryllium	100	9	ng m^{-3}	0.002	0.003	−0.003	0.000	0.002	0.004	0.013
Bismuth	100	209	ng m^{-3}	0.008	0.010	−0.001	0.001	0.004	0.012	0.057
Cadmium	100	114	ng m^{-3}	0.040	0.126	0.000	0.006	0.015	0.036	0.992
Calcium	100	40	ng m^{-3}	45.81	39.29	−0.67	12.54	36.24	65.10	191.23
Cerium	100	140	ng m^{-3}	0.054	0.047	0.003	0.018	0.046	0.076	0.230
Cesium	100	133	ng m^{-3}	0.006	0.006	0.000	0.002	0.004	0.008	0.032
Chromium	100	52	ng m^{-3}	0.267	0.351	−0.047	0.039	0.167	0.325	1.944
Cobalt	100	59	ng m^{-3}	0.012	0.014	−0.009	0.001	0.009	0.020	0.053
Copper	100	63	ng m^{-3}	1.192	2.261	−0.106	0.105	0.458	0.997	13.304
Iron	100	56	ng m^{-3}	46.10	40.04	−0.88	12.71	36.26	67.80	183.11
Lanthanum	100	139	ng m^{-3}	0.025	0.022	0.001	0.007	0.020	0.035	0.115
Lead	100	208	ng m^{-3}	0.393	0.498	0.000	0.094	0.224	0.455	3.389
Lithium	100	7	ng m^{-3}	0.048	0.038	0.000	0.021	0.039	0.064	0.170
Magnesium	100	26	ng m^{-3}	14.80	16.06	0.60	4.51	11.88	17.15	104.74
Manganese	100	55	ng m^{-3}	1.282	1.279	−0.011	0.455	1.060	1.560	9.792
Molybdenum	100	98	ng m^{-3}	0.043	0.072	−0.008	0.006	0.024	0.046	0.466
Neodymium	100	143	ng m^{-3}	0.023	0.020	0.001	0.007	0.017	0.031	0.094
Nickel	100	60	ng m^{-3}	0.584	4.568	−0.049	0.018	0.095	0.190	45.782
Niobium	100	93	ng m^{-3}	0.006	0.006	−0.001	0.001	0.004	0.010	0.029
Phosphorus	29	31	ng m^{-3}	6.65	9.02	0.00	0.00	0.00	10.70	36.27
Platinum	100	195	ng m^{-3}	0.001	0.001	−0.001	0.000	0.001	0.002	0.004
Potassium	100	39	ng m^{-3}	38.8	49.0	1.5	15.7	26.3	40.7	328.0
Praseodymium	100	141	ng m^{-3}	0.007	0.005	0.000	0.003	0.006	0.010	0.025
Rubidium	100	85	ng m^{-3}	0.113	0.133	−0.002	0.039	0.085	0.127	0.953
Samarium	100	147	ng m^{-3}	0.005	0.004	0.000	0.002	0.004	0.007	0.018
Selenium	100	78	ng m^{-3}	0.088	0.274	0.000	0.027	0.053	0.076	2.770
Silicon	100	28	ng m^{-3}	88.7	96.4	−21.1	12.0	77.0	140.7	391.5
Sodium	100	23	ng m^{-3}	28.3	60.1	−3.5	2.0	8.8	22.1	415.3
Strontium	100	88	ng m^{-3}	0.236	0.218	−0.022	0.067	0.203	0.314	1.122
Sulfur (XRF)	100	–	ng m^{-3}	378.8	251.8	24.7	177.3	305.1	539.9	1194.1
Tantalum	100	181	ng m^{-3}	0.001	0.001	0.000	0.000	0.001	0.002	0.003
Thallium	100	205	ng m^{-3}	0.004	0.004	0.000	0.002	0.003	0.006	0.025
Thorium	100	232	ng m^{-3}	0.007	0.007	0.000	0.002	0.006	0.010	0.037
Tin	100	118	ng m^{-3}	0.100	0.119	0.000	0.045	0.075	0.113	1.009
Titanium	100	49	ng m^{-3}	1.970	2.021	−0.161	0.446	1.376	2.768	9.650
Tungsten	100	182	ng m^{-3}	0.010	0.011	−0.003	0.002	0.006	0.013	0.061
Uranium	100	238	ng m^{-3}	0.003	0.003	0.000	0.001	0.002	0.004	0.014
Vanadium	100	51	ng m^{-3}	0.253	0.413	−0.007	0.047	0.149	0.287	2.841
Zinc	100	68	ng m^{-3}	4.376	11.414	−0.843	0.318	1.922	3.931	105.79

sampler was operational. The run time associated with these invalidated samples ranged from 4.3–15.8 h (8.5 ± 5). The $PM_{2.5}$ and $PM_{10-2.5}$ results associated with the Richardson fire impacted samples that ran <23 h (n = 7) during the study period are summarized in Table 2 and represent extremely high ambient concentrations. Two valid pairs of Richardson wildland fire impacted dichotomous samples were collected during this time frame on May 29 ($PM_{2.5}$ = 143.4 μg m^{-3}) and May 30, 2015 ($PM_{2.5}$ = 170.5 μg m^{-3}).

A subset of 100 dichotomous sample pairs from the valid population of 392 sample pairs was selected for element analysis and source apportionment modeling. The selected samples included an even distribution across the seasons and the two valid wildland fire impacted samples. The statistical summary of the selected sample $PM_{2.5}$ (8.6 ± 21.6 μg m^{-3}) and $PM_{10-2.5}$ (7.6 ± 5.9 μg m^{-3}) sample pair mass concentrations are presented in Table 1. A statistical summary of the ED-XRF and DRC-ICPMS analytical results of the selected samples are presented in Tables 3 and 4 for $PM_{2.5}$ and $PM_{10-2.5}$, respectively.

3.3. $PM_{2.5}$ PMF source apportionment results

Pearson correlation coefficients were calculated for all measured chemical species with measured $PM_{10-2.5}$ and $PM_{2.5}$ mass to investigate relationships that might result in factors resolved by the PMF model. Overall, $PM_{2.5}$ mass was found to be moderately correlated with most of the chemical constituents (r^2 = 0.3–0.6), while $PM_{10-2.5}$ mass displayed stronger correlations (r^2 = 0.6–0.9). Elements Ba, Be, Bi, Cr, Cu, Mg, Na, Pd, Pt, Sb, Sn, Ta, Th, U in the $PM_{2.5}$ fraction, and Bi, Cd, Cu, Pd, Pt, Sn in the $PM_{10-2.5}$ fraction did not exhibit statistically significant correlation with the measured mass at 5% significance level. As noted below, because of this result and other factors, several of these elements were not used in the PMF analysis.

After careful evaluation of the data set and several iterative runs varying the number of factors from 3 to 7, a 5-factor solution with 32 species was found to be optimal. Rotational ambiguity was explored by varying the "fpeak" parameter between −0.5 and 1.0. Overall, insignificant changes (<5%) in contribution estimates were observed. Zero fpeak was preferred for further analyses, as this is most likely to be physically meaningful (Paatero et al., 2002). The PMF solution was further evaluated using BBS to determine the error estimates associated with the factor profiles. Results showed minor instability in the factors later identified as winter road salt and the Pb factor. After 100 BBS uncertainty analysis runs, eleven runs for these two factors were unmapped. Temporal source contribution estimate (SCE) analysis of both the winter road salt and lead profiles shows seasonal contributions and a relatively limited number of overall samples contributing to these factors. Creation of random datasets by the BBS procedure sometimes undercounted samples representing these two factors because of their seasonality dependence. Bootstrap elemental profile

Table 4
Statistical summary of mass and trace elements in ambient $PM_{10-2.5}$.

Analyte	n	Isotope	Unit	Mean	Std. Dev.	Min	Q1	Median	Q3	Max
$PM_{10-2.5}$ mass	100	–	μg m^{-3}	7.56	5.88	0.48	3.12	6.53	10.74	26.38
Aluminum	100	27	ng m^{-3}	300.5	261.7	0.0	76.8	254.7	406.2	1159.6
Antimony	100	123	ng m^{-3}	0.023	0.029	−0.013	0.007	0.015	0.030	0.216
Arsenic oxide	100	91	ng m^{-3}	0.072	0.061	0.001	0.025	0.062	0.098	0.268
Barium	100	137	ng m^{-3}	2.732	2.482	−1.613	0.733	2.392	4.166	9.785
Beryllium	100	9	ng m^{-3}	0.009	0.008	−0.004	0.003	0.008	0.013	0.034
Bismuth	100	209	ng m^{-3}	0.003	0.004	−0.001	0.001	0.002	0.004	0.029
Cadmium	100	114	ng m^{-3}	0.011	0.086	−0.008	0.001	0.002	0.003	0.866
Calcium	100	40	ng m^{-3}	387.0	390.0	0.0	84.2	261.0	601.8	1777.8
Cerium	100	140	ng m^{-3}	0.343	0.294	0.000	0.100	0.300	0.476	1.420
Cesium	100	133	ng m^{-3}	0.023	0.020	0.000	0.007	0.019	0.030	0.094
Chromium	100	52	ng m^{-3}	1.062	0.844	0.000	0.430	0.859	1.496	3.586
Cobalt	100	59	ng m^{-3}	0.095	0.077	0.001	0.029	0.079	0.135	0.316
Copper	100	63	ng m^{-3}	1.082	1.926	−0.774	0.203	0.520	1.296	16.473
Iron	100	56	ng m^{-3}	311.6	289.0	0.5	86.2	251.0	448.7	1416.1
Lanthanum	100	139	ng m^{-3}	0.170	0.144	0.000	0.052	0.152	0.243	0.686
Lead	100	208	ng m^{-3}	0.136	0.122	−0.003	0.049	0.101	0.196	0.640
Lithium	100	7	ng m^{-3}	0.281	0.233	−0.002	0.073	0.251	0.389	1.003
Magnesium	100	26	ng m^{-3}	66.41	57.98	0.02	19.72	55.27	92.84	290.36
Manganese	100	55	ng m^{-3}	6.036	7.429	−0.043	1.482	4.374	7.669	55.564
Molybdenum	100	98	ng m^{-3}	0.050	0.044	−0.006	0.017	0.040	0.068	0.266
Neodymium	100	143	ng m^{-3}	0.147	0.125	0.000	0.041	0.128	0.193	0.534
Nickel	100	60	ng m^{-3}	0.405	0.429	−0.112	0.103	0.290	0.550	2.489
Niobium	100	93	ng m^{-3}	0.045	0.039	0.000	0.012	0.035	0.065	0.190
Phosphorus	29	31	ng m^{-3}	15.43	10.13	2.58	8.07	13.57	16.58	44.83
Platinum	100	195	ng m^{-3}	0.001	0.002	−0.001	0.000	0.002	0.002	0.012
Potassium	100	39	ng m^{-3}	94.91	76.43	−5.21	33.44	84.04	131.48	325.80
Praseodymium	100	141	ng m^{-3}	0.040	0.033	0.000	0.011	0.034	0.053	0.142
Rubidium	100	85	ng m^{-3}	0.416	0.358	−0.007	0.125	0.377	0.612	1.784
Samarium	100	147	ng m^{-3}	0.028	0.023	0.000	0.008	0.024	0.037	0.099
Selenium	100	78	ng m^{-3}	0.105	0.084	−0.001	0.038	0.090	0.157	0.383
Silicon	100	28	ng m^{-3}	892.6	785.2	2.9	230.5	686.0	1418.9	3882.9
Sodium	100	23	ng m^{-3}	37.25	42.91	−1.74	11.03	24.45	51.69	289.63
Strontium	100	88	ng m^{-3}	1.216	1.088	−0.017	0.358	1.001	1.623	4.969
Sulfur (XRF)	100	–	ng m^{-3}	44.85	34.73	−3.50	23.34	38.41	56.96	244.71
Tantalum	100	181	ng m^{-3}	0.005	0.006	0.000	0.002	0.003	0.006	0.055
Thallium	100	205	ng m^{-3}	0.004	0.003	−0.001	0.002	0.004	0.006	0.014
Thorium	100	232	ng m^{-3}	0.048	0.040	0.000	0.014	0.039	0.068	0.179
Tin	100	118	ng m^{-3}	0.030	0.020	−0.013	0.018	0.031	0.041	0.130
Titanium	100	49	ng m^{-3}	13.65	12.44	0.06	3.53	10.30	19.84	58.17
Tungsten	100	182	ng m^{-3}	0.036	0.041	−0.001	0.011	0.023	0.047	0.232
Uranium	100	238	ng m^{-3}	0.013	0.011	0.000	0.004	0.012	0.019	0.048
Vanadium	100	51	ng m^{-3}	0.810	0.660	−0.014	0.247	0.706	1.211	2.903
Zinc	100	68	ng m^{-3}	1.879	1.751	−0.557	0.779	1.640	2.567	13.284

concentrations whose 5th percentile concentrations were greater than zero, were considered as significantly different from zero, and used in interpreting factors.

Figs. 4 and 5 present $PM_{2.5}$ PMF factor profiles as percent mass explained and temporal SCE for each factor, respectively. Factor 1 explained over 70% of the Al, Ca, Ce, Fe, La, Nb, Nd, Si, Sm, and Ti suggesting predominance of a crustal element source. The temporal variability trend (Fig. 5a) shows an extremely low contribution of this factor in the winter when the ground is frozen and often covered with snow, and highest in the spring and fall when the local wind speeds are seasonally high. In combination, the chemistry and temporal characteristics of this factor are indicative of a fine fraction fugitive dust source.

Factor 2 explained 97% of the measured Pb concentrations. Other elements with significant loading on this factor are As (27%), Cs (32%), Zn (15%), and Cd (17%). Lead can be emitted into the atmosphere by several high temperature anthropogenic sources such as non-ferrous metal smelting, battery recycling, coal combustion, waste incineration, and piston aircraft operating on leaded aviation fuel (U.S. EPA, 2015). Once emitted, lead may be transported on local, regional, or intercontinental scales depending on various factors, including particle size, the elevation of emission, and meteorology. The PMF lead factor demonstrates a seasonal temporal trend (Fig. 5b) with two primary episodes observed during the spring of 2010 and the spring of 2011. This seasonal pattern is not correlated with known emissions from local or regional sources,

Fig. 4. PMF $PM_{2.5}$ source profiles (% attributed mass).

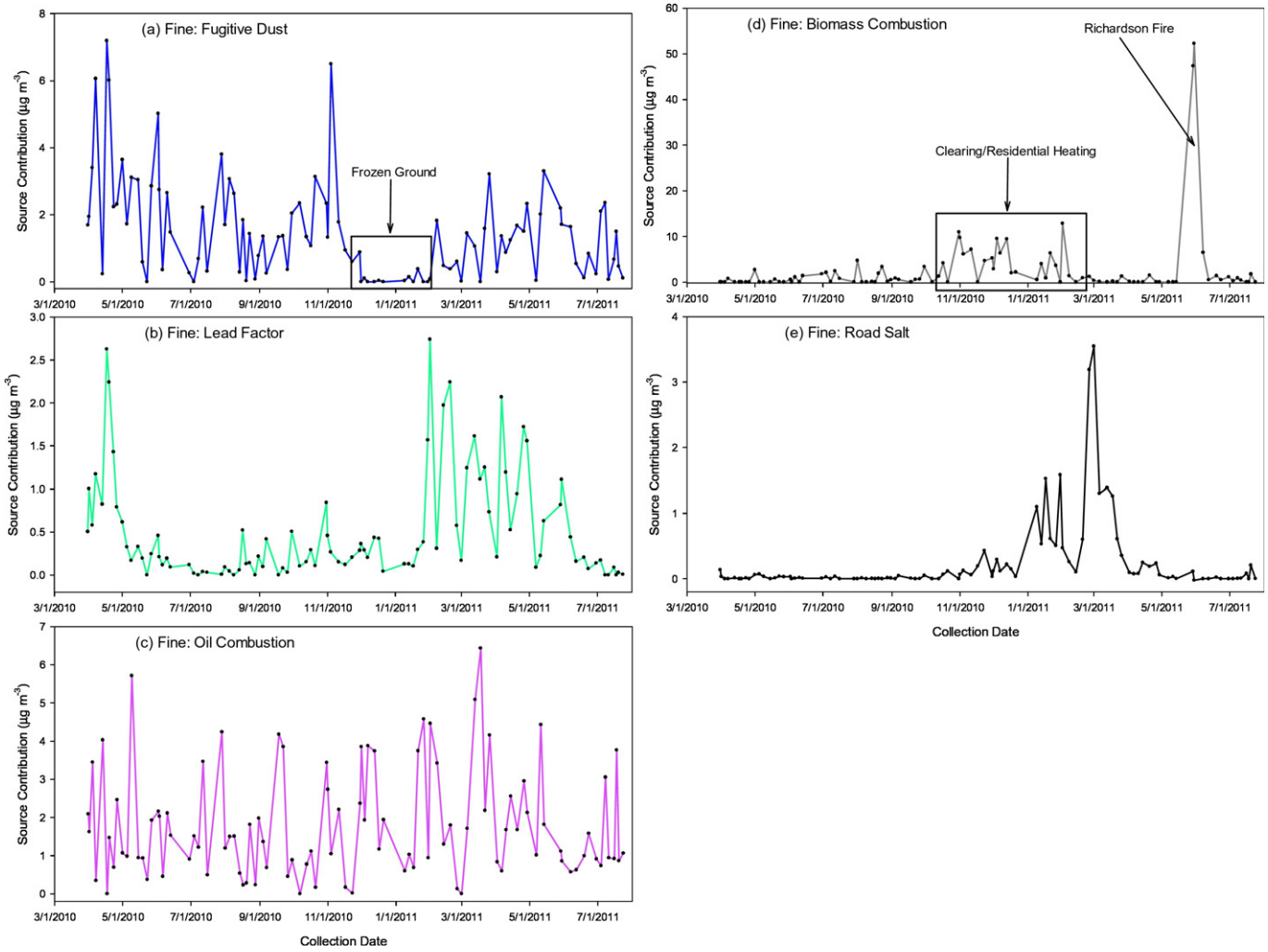

Fig. 5. PMF $PM_{2.5}$ source contribution estimate time series.

but is consistent with previously observed trans-Pacific transport of pollution from Asia to western North America (Yienger et al., 2000; VanCuren and Cahill, 2002; VanCuren, 2003; Gallon et al., 2011). Graney et al. (2017a) analyzed all the dichotomous sampler filter extracts from this study for stable Pb isotopic ratios, and found that the ratios associated with many of these spring episodes are consistent with lead of Asian origin. We therefore characterize the lead factor as an Asian long-range transported source.

Factor 3 is characterized by SO_2, S, Mo, V, and Ni with negligible crustal element contributions. All of these species are known markers of oil production processes or oil combustion. The presence of V, Ni, and La, with La/V < 0.1 likely indicates Factor 3 is an oil combustion/bitumen upgrading source (Olmez and Gordon, 1985; Ondov and Wexler, 1998; Kulkarni et al., 2007; Landis et al., 2012). The temporal pattern of the PMF source contribution estimates (SCEs) for the oil production/combustion factor depicted in Fig. 5c shows relatively steady contributions regardless of season, which reflects the continuous nature of both the mining fleet and upgrading operations in the region.

Factor 4 is characterized by As (40%), Cd (83%), K (76%), Rb (58%), Zn (73%), NO_x (27%), and ammonia (100%) concentrations, and represents biomass combustion. Six of the seven invalid samples collected during the Richardson backcountry wildland fire events (May 18 – June 15, 2011) where the dichotomous sampler shut off due to extreme filter loading were included in the model to help PMF establish the profile for this source but were not included in the mass apportionment. These same samples were used by Landis et al. (2012) to establish a wildland fire source profile in the AOSR. The influence of the three valid Richardson wildland fire event samples is clearly evident in Fig. 5d. The presence of the higher biomass combustion SCEs from November 2010 through February 2011 indicates a significant $PM_{2.5}$ contribution from biomass burning from land clearing operations at future oil sand mine locations and local residential wood combustion for home heating.

Factor 5 is characterized by high loadings for Na (100%), NO_x (72%), and Mg (32%). This source contribution is only appreciable during the winter months, suggesting that this factor represents resuspended road salt (NaCl, MgCl) from applied deicing materials. The elevated NO_x associated with this source is indicative of mobile source contributions during periods when nocturnal inversions, low boundary layer heights, and seasonally low winds speeds are typical in the AOSR.

3.4. $PM_{10-2.5}$ PMF source apportionment results

A six-factor $PM_{10-2.5}$ PMF solution utilizing the same 32 species as the $PM_{2.5}$ model run was found to be optimal both in terms of explained variance and model fit statistics (Fig. 6). Of the 100 bootstrap runs, the factor identified as mixed source fugitive dust was correctly mapped in only 84% of the runs, whereas other factors were mapped to their base factors in ≥96% of the runs.

Factor 1 showed significant loadings for Ba (58%), Zn (69%), Fe (9%), and Mg (6%). These elements have been associated with coarse fraction brake and tire wear particulate emissions in other studies (Garg et al.,

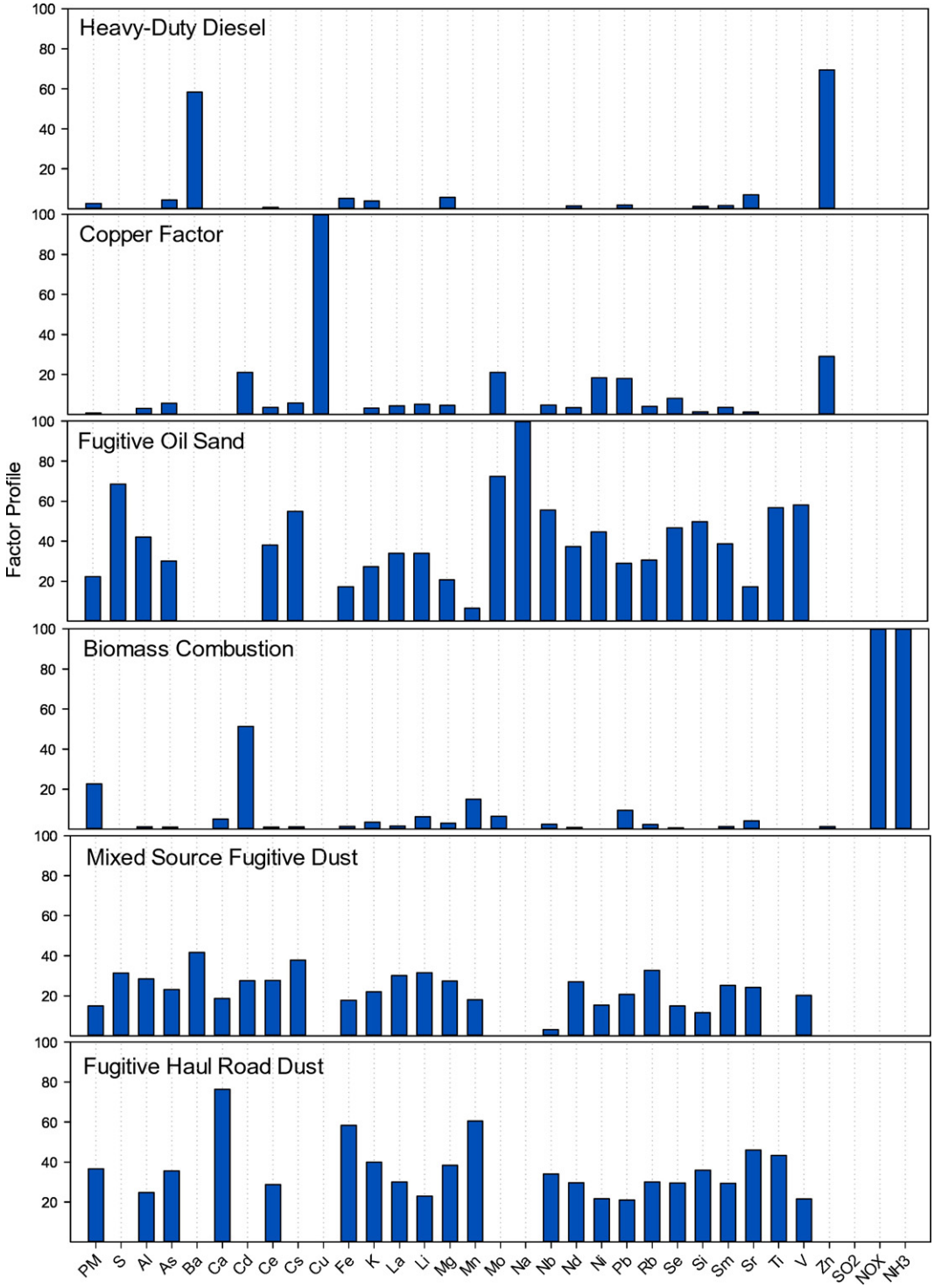

Fig. 6. PMF $PM_{10-2.5}$ source profiles (% Attributed Mass).

2000; Wik and Dave, 2009; Gietl et al., 2010; Kreider et al., 2010; Grigoratos and Martini, 2015). Ba and Zn are also found in diesel fuel in the AOSR (Landis et al., 2012). Tire wear is likely to result in predominantly carbonaceous particles, although small quantities of metals, in particular Zn that is used as a vulcanization activator, may be present (Wik and Dave, 2009). Therefore, this factor was identified as a mobile source factor. The SCE temporal trend (Fig. 7a) did not show weekday/weekend trends typical of commuter traffic sources in urban areas. Rather, since oil sands mining and processing is continuous, emissions from local road traffic and heavy-duty hauler fleets were also expected to be continuous as these SCE results suggest.

Factor 2 is primarily driven by Cu (100%) with contributions of other trace metals such as Cd (21%), Mo (21%), Ni (18%), Pb (18%), and Zn (29%). The Cu measurement data was peculiar in the sense that despite exhibiting temporal concentration excursions (Fig. 7b), it did not show any significant association with either $PM_{2.5}$ or $PM_{10-2.5\ mass}$ at the 5% confidence level. Studies have identified contamination of PM samples particularly with Cu through the collection of aerosols from the exhaust

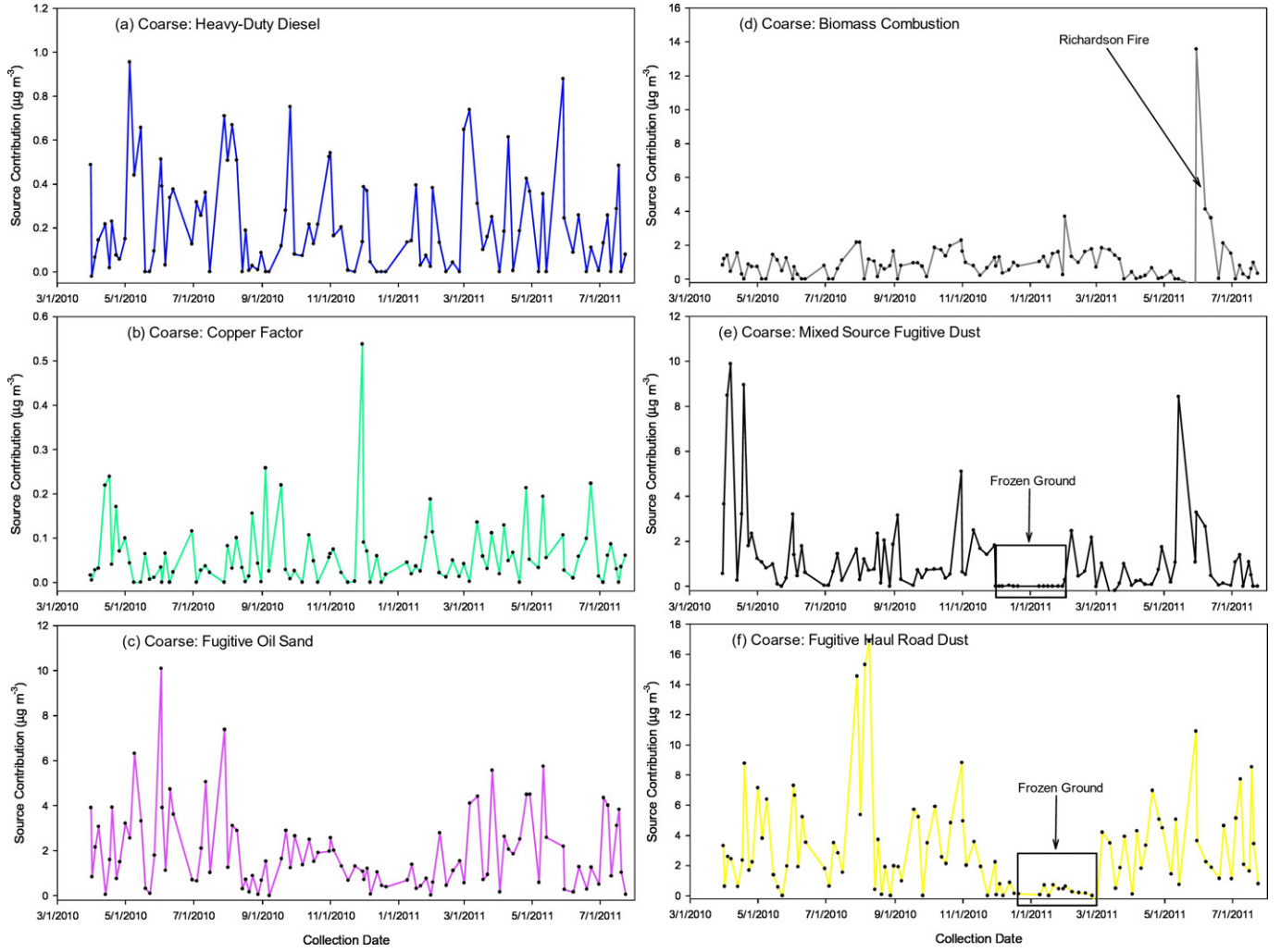

Fig. 7. PMF $PM_{10-2.5}$ source contribution estimate time series.

from other air sampler motors at the monitoring site, especially from carbon vein pump exhaust (Patterson, 1980; Pancras and Landis, 2011). WBEA operated several high volume air samplers at the Fort McKay site equipped with carbon vein pumps during this study period as part of the Environment Canada National Air Pollution Surveillance Program (NAPS). Even though each of these samplers were equipped with pump exhaust tubes that directed the exhaust away from the monitoring site, the synchronicity of the factor impacts with the high volume sampler operating schedule at the AMS-1 site highlights their potential impact on the sequential dichotomous samples. Thus, this factor is regarded as a Cu contamination source.

Factor 3 is loaded with elements associated with both (i) bitumen V (58%), Ni (45%), S (69%), Se (47%), Mo (72%) and (ii) sand Si (50%), Al (42%), and Ti (57%). The factor profile concentrations closely resembles the oil sand source profile published by Landis et al. (2012) using oil sand grab sample profiles (Appendix Fig. B.3), suggesting that this factor likely represents resuspended oil sand in fugitive dust. The highest SCE estimates for this source (Fig. 7c) are observed in the spring and summer when meteorological conditions (e.g., high winds) and dry surface conditions favor the suspension of fugitive dust from mining and hauling operations.

Factor 4 is predominantly driven by NH_3 (100%) and Cd (51%) with minor contributions from K (4%) and Mn (15%). This factor is thought to be representative of biomass smoke and biomass combustion ash. Contributions from this factor can be dominant during known wildland fire episodes and during the winter (home heating and biomass burning from land clearing operations), but are discernible year round (Fig. 7d).

Factors 5 and 6 are quite similar in terms of emission profiles with the exception of a few key tracer species, but differed in temporal contribution profiles in non-winter months. Both sources have near-zero contributions in the winter (Fig. 7e &f) when the ground is frozen and often covered with snow, suggesting fugitive dust sources for these two factors. Crustal element markers are present in both factors but with higher relative abundance in Factor 6. The Ca (76%), Fe (58%), Mg (38%), Mn (60%), Si (36%), and Sr (46%) profile abundance in Factor 6 indicates the presence of limestone and resembles the haul road source profiles (Appendix Fig. B.3). The mined limestone in the AOSR is used along with low-grade oil sand to construct temporary roads for heavy-duty hauler traffic. Therefore, this factor is regarded as resuspended haul road dust. Factor 5 differs from the fugitive haul road dust factor with (i) loadings of S, Ba, Cd, and Cs, (ii) the absence of Ti, and (iii) reduced loading of Ca. It is thought that this factor represents a mixed fugitive dust source that coincidentally is very similar to the temporal distribution and chemical composition of the fine fraction fugitive dust source (Figs. 5a and 7e). This coincidence is likely related to the size distribution of clay mineral particles in the AOSR (Graney et al., 2017b) that likely overlaps the $PM_{2.5}$ and $PM_{10-2.5}$ collection cut point in the dichotomous sampler. Clay minerals and clay-sized particles (by definition <2 µm in diameter) in the AOSR are composed mainly of kaolinite ($Al_2Si_2O_5(OH)_4$) with greater amounts of silt and sand sized

Table 5
$PM_{2.5}$ mass apportioned to identified sources, with all data and the two wildland fire events excluded scenarios.

Source	No wildland fire-impacted samples (n = 98)		All samples (n = 100)	
	Mean	Explained	Mean	Explained
Oil combustion	1.80	32%	1.78	21%
Fugitive dust	1.44	26%	1.45	17%
Biomass combustion	1.38	25%	2.35	27%
Lead factor	0.49	9%	0.50	6%
Road salt	0.23	4%	0.22	3%
Unexplained	0.26	4%	2.31	26%
$PM_{2.5}$ mass (μg m^{-3})	5.61		8.64	

grains (predominantly quartz – SiO_2) in the coarser size fractions (Osacky et al., 2013; Graney et al., 2017b). Mixtures of these minerals are reflected in the Si/Al ratios in source and particulate matter samples. For example based on the PMF source contribution profiles, the average Si/Al in the fine fraction fugitive dust is 2.3 whereas in the coarse particulate matter the oil sand fugitive dust ratio is 3.4, haul road fugitive dust is 4.1 and the mixed source fugitive dust is 1.2. The lowest Si/Al ratio in the mixed source fugitive dust factor suggests a greater contribution from minerals such as kaolinite. This mixed source fugitive dust factor likely contains clay mineral contributions from overburden removal, tailings ponds, and petroleum coke stockpiles (Landis et al., 2012) as well as from oil sand and haul roads.

3.5. Particulate matter mass apportionment

Of the average $PM_{2.5}$ mass concentration of 8.6 μg m^{-3}, 74% was explained by the 5 factor fine PM model when the two highest wildland fire samples were included (Table 5). However, the explained mass increased to 96% and the mean $PM_{2.5}$ mass concentration decreased to 5.6 μg m^{-3} when the two highest wildland fire impact days were excluded. In general, PMF will underestimate high concentration outlier events, leading to the increased overall model uncertainty (Pancras et al., 2011). Appendix Fig. B.4 presents the PMF $PM_{2.5}$ apportioned versus observed mass for all the samples including the Richardson wildfire smoke impacted samples, which are poorly reproduced by PMF. In the case of the model excluding the seven invalid and two valid highly wildland fire impacted samples, oil combustion/upgrading was the largest contributor (32%), followed by fugitive dust (26%), biomass combustion (25%), long range transported industrial lead source (9%), and winter road salt (4%). The relatively large contribution of biomass burning despite the two wildland fire events removed is likely due to residential wood combustion for home heating, and brush burning from land clearing activities.

The impact of the two wildland fire impacted samples on $PM_{10-2.5}$ PMF apportionment results appeared minor. The percentages of unexplained mass with and without wildfire samples were 2.4 and 1.2%, respectively (Table 6). The three anthropogenic fugitive dust factors explained in excess of 80% of the $PM_{10-2.5}$ mass in Fort McKay, which is consistent with monitoring site location proximity to three large oil sand surface mining operations. Fugitive haul road dust was the largest contributor (40%), followed by fugitive dust from oil sand (26%), mixed source fugitive dust (15%), biomass combustion (13%), and mobile source brake and tire wear emissions (3%). Abatement strategies targeting the three major types of fugitive dust would likely result in significant reductions in ambient $PM_{10-2.5}$ concentrations in the Fort McKay community.

Table 6
$PM_{10-2.5}$ mass apportioned to identified sources, with all data and the two wildland fire events excluded scenarios.

Source	No wildland fire-impacted samples (n = 98)		All samples (n = 100)	
	Mean	Explained	Mean	Explained
Fugitive haul road	2.93	40%	3.02	40%
Fugitive oil sand	1.95	27%	1.94	26%
Mixed fugitive	1.14	16%	1.16	15%
Biomass combustion	0.87	12%	0.98	13%
Mobile source	0.20	3%	0.21	3%
Copper factor	0.06	1%	0.06	1%
Unexplained	0.09	1%	0.18	2%
PM_{10} mass (μg m^{-3})	7.26		7.57	

4. Conclusions

An intensive ambient particulate matter monitoring study was conducted in the Fort McKay First Nations Community, which is located in close proximity to several oil sand mining and bitumen upgrading operations in northern Alberta, Canada. Running from February 2010 to July 2011, the study found almost equal concentrations of $PM_{2.5}$ (6.8 ± 12.9 μg m^{-3}) and $PM_{10-2.5}$ (6.9 ± 5.9 μg m^{-3}) in the community. Source apportionment modeling found that approximately 58% of the observed $PM_{2.5}$ and 83% of the observed $PM_{10-2.5}$ was attributable to local anthropogenic emissions related to oil sands production operations. An additional 25% of the observed $PM_{2.5}$ was attributed to biomass combustion, even after the Richardson Backcountry wildfire event impacted samples were removed from the analysis, highlighting the influence of residential wood heating and land clearing burning operations. The estimated overall contribution of fugitive dust emissions during this study was found to be consistent with source apportionment estimates reported from a regional scale resolved epiphytic lichen bioindicator study (Landis et al., 2012). Results from this study also show significant temporal variability in source contributions, including: (i) fugitive dust contributions with minimal impacts in the winter when the ground, haul roads, overburden and byproduct stockpiles, and mine faces were frozen and often covered in snow; (ii) oil combustion and heavy hauler emission contributions show no significant seasonal trend; (iii) Asian lead dust contributions peak in the spring, when synoptic meteorological conditions are favorable for long-range transport; and (iv) biomass combustion impacts were highest in the summer during wildland fire season, but also contributed significantly during the winter when brush burning operations and residential wood heating is common.

Acknowledgements

This work was funded by the Wood Buffalo Environmental Association (WBEA). The content and opinions expressed by the authors do not necessarily reflect the views of the WBEA or of the WBEA membership. We thank Gary Cross (WBEA) for managing the ambient sample collection activities in the AOSR; Sanjay Prasad (WBEA) for providing AMS-1 Fort McKay monitoring site ancillary ambient measurement data used in our analysis; Zack Eastman, Hayley Drake, and Kendra Thomas (WBEA) for ambient sample support; Karsten Baumann (ARA) for logistical support, Brad Edgerton (ARA) for filter weighing, and Mike Fort (ARA) for dichotomous sampler filter extraction and ED-XRF and DRC-ICPMS analysis.

Appendix A. Supplementary Information

Supplementary data to this article can be found online at http://dx.doi.org/10.1016/j.scitotenv.2017.01.110.

References

Alberta Energy, 2017. Facts and Figures. http://www.energy.alberta.ca/OilSands/791.asp (Last Accessed January 24, 2017).

Attanasi, E.D., Meyer, R.F., 2010. Natural Bitumen and Extra-heavy Oil - Survey of Energy Resources. 22 ed. World Energy Council, pp. 123–140 (ISBN 0-946121-26-5).
Edgerton, E.S., Fort, J.M., Baumann, K., Graney, J.R., Landis, M.S., Berryman, S., Krupa, S., 2012. Method for extraction and multi-element analysis of *Hypogymnia physodes* samples from the Athabasca Oil Sands Region. In: Percy, Kevin (Ed.), Alberta Oil Sands: Energy, Industry and the Environment. Elsevier, Oxford, England, pp. 315–342.
Gallon, C., Ranville, M.A., Conaway, C.H., Landing, W.M., Buck, C.S., Morton, P.L., Flegal, A.R., 2011. Asian industrial lead inputs to the north Pacific evidenced by lead concentrations and isotopic compositions in the surface waters and aerosols. Environ. Sci. Technol. 45, 9874–9882.
Garg, B., Cadle, S.H., Mulawa, P.A., Groblicki, P.J., Laroo, C., Parr, G.A., 2000. Brake wear particulate matter emissions. Environ. Sci. Technol. 34, 4463–4469.
Gietl, J.K., Lawrence, R., Thorpe, A.J., Harrison, R.M., 2010. Identification of brake wear particles and derivation of a quantitative tracer for brake dust at a major road. Atmos. Environ. 44, 141–146.
Government of Alberta (Ed.), March 2008l. Alberta's Oil Sands: Opportunity, Balance (ISBN 978-0-7785-7348-7).
Graney, J.R., Landis, M.S., Edgerton, E.S., 2017a. Using lead isotope ratios and multi-element analysis from Fort McKay, Alberta, Canada ambient fine and coarse fraction particulate matter to identify local, regional, and global scale emission sources. Atmos. Environ. (In Review).
Graney, J.R., Landis, M.S., Puckett, K.J., Studabaker, W., Edgerton, E.S., Legge, A., Percy, K.E., 2017b. Differences in accumulation of PAHs, elements, and Pb isotopes by five lichen species in the world's largest oil sands production region. Chemosphere (In Review).
Grigoratos, T., Martini, G., 2015. Brake wear particle emissions: a review. Environ. Sci. Pollut. Res. Int. 22, 2491–2504.
Hopke, P.K., 2009. Theory and application of atmospheric source apportionment. In: Legge, A.H. (Ed.), Air Quality and Ecological Impacts. Elsevier, Amsterdam, The Netherlands.
Hopke, P.K., 2016. A review of receptor modeling methods for source apportionment. J. Air Waste Manage. Assoc. 66, 237–259.
Jalkanen, L.M., Häsänen, E.K., 1996. Simple method for the dissolution of atmospheric aerosol samples for analysis by inductively coupled plasma mass spectrometry. J. Anal. At. Spectrom. 11, 365–369.
Kreider, M.L., Panko, J.M., McAtee, B.L., Sweet, L.I., Finley, B.L., 2010. Physical and chemical characterization of tire-related particles: comparison of particles generated using different methodologies. Sci. Total Environ. 408, 652–659.
Kulkarni, P., Chellam, S., Fraser, M.P., 2007. Tracking petroleum refinery emission events using lanthanum and lanthanides as elemental markers for $PM_{2.5}$. Environ. Sci. Technol. 41, 6748–6754.
Landis, M.S., Pancras, J.P., Graney, J.R., Stevens, R.K., Percy, K.E., Krupa, S., 2012. Receptor modeling of epiphytic lichens to elucidate the sources and spatial distribution of inorganic air pollution in the Athabasca Oil Sands Region. In: Percy, Kevin (Ed.), Alberta Oil Sands: Energy, Industry and the Environment. Elsevier, Oxford, England, pp. 427–467.
Loo, B.W., Cork, C.P., 1988. Development of high efficiency virtual impactors. Aerosol Sci. Technol. 9, 167–176.
Masliyah, J., Zhou, Z., Xu, Z., Czarnecki, J., Hamza, H., 2004. Understanding water-based bitumen extraction from Athabasca Oil Sands. Can. J. Chem. Eng. 82, 628–654.
Olmez, A.E., Gordon, G.E., 1985. Rare earths: atmospheric signatures for oil-fired power plants and refineries. Science 6, 966–968.
Ondov, J.M., Wexler, A.S., 1998. Where do particulate toxins reside? An improved paradigm for the structure and dynamics of the urban mid-Atlantic aerosol. Environ. Sci. Technol. 32, 2547–2555.
Osacky, M., Geramian, M., Ivey, D.G., Liu, Q., Etsell, T.H., 2013. Mineralogical and chemical composition of petrologic end members of Alberta Oil Sands. Fuel 113, 148–157.
Paatero, P., 1999. The multilinear engine — a table-driven least squares program for solving multilinear problems, including the n-way parallel factor analysis model. J. Comput. Graph. Stat. 8, 854–888.
Paatero, P., Hopke, P.K., Song, X.H., Ramadan, Z., 2002. Understanding and controlling rotations in factor analytic models. Chemom. Intell. Lab. 60, 253–264.
Pancras, J.P., Landis, M.S., 2011. Performance Evaluation of modified Semi-continuous Elements in Aerosol Sampler-III. Atmos. Environ 45, 6751–6759.
Pancras, J.P., Vedantham, R., Landis, M.S., Norris, G.A., Ondov, J.M., 2011. Application of EPA unmix and nonparametric wind regression on high time resolution trace elements and speciated mercury in Tampa, Florida. Environ. Sci. Technol. 45, 3511–3518.
Pancras, J.P., Landis, M.S., Norris, G.A., Vedantham, R., Dvonch, J.T., 2013. Source apportionment of ambient fine particulate matter in Detroit, Michigan, using hourly resolved PM chemical composition data. Sci. Total Environ. 448, 2–13.
Patterson, R.K., 1980. Aerosol contamination from high-volume sampler exhaust. J. Air Pollut. Control Assoc. 30 (2), 169–171.
Solomon, P.A., Norris, G.A., Landis, M.S., Tolocka, M., 2001. Chemical analysis methods for atmospheric aerosol components. In: Baron, P.A., Willeke, K. (Eds.), Aerosol Measurement. John Wiley & Sons, Inc., pp. 261–293.
U.S. Environmental Protection Agency, Nov 2011. EPA Positive Matrix Factorization (PMF) 4.2 Fundamentals & User Guide. Report No. EPA-600/R-11/117. Office of Research and Development, Washington, DC, USA.
U.S. Environmental Protection Agency, March 2015. The 2011 National Emissions Inventory, Version 2. Office of Air Quality Planning and Standards, Research Triangle Park, NC, USA (Last Accessed April 1, 2016. https://www3.epa.gov/ttn/chief/net/2011inventory.html).
VanCuren, R.A., 2003. Asian aerosols in North America: extracting the chemical composition and mass concentration of the Asian continental aerosol plume from long-term aerosol records in the western United States. J. Geophys. Res. Atmos. 108, 4263.
VanCuren, R.A., Cahill, T.A., 2002. Asian aerosols in North America: frequency and concentration of fine dust. J. Geophys. Res. 107, 4804.
Wang, X., Chow, J.C., Kohl, S.D., Percy, K.E., Legge, A.H., Watson, J.G., 2015. Characterization of $PM_{2.5}$ and PM_{10} fugitive dust source profiles in the Athabasca Oil Sands Region. J. Air Waste Manage. Assoc. 65, 1421–1433.
Wang, X., Chow, J.C., Kohl, S.D., Percy, K.E., Legge, A.H., Watson, J.G., 2016. Real-world emission factors for Caterpillar 797B heavy haulers during mining operations. Particuology 28, 22–30.
Wik, A., Dave, G., 2009. Occurrence and effects of tire wear particles in the environment - a critical review and an initial risk assessment. Environ. Pollut. 157, 1–11.
Wood Buffalo Environmental Association, 2011. Annual Report – Continuous Monitoring, March 10, 2012. (Last accessed April 1, 2016. http://wbea.org/resources/ambient-air-monitoring-reports/ambient-annual-reports).
World Health Organization, 1980. Analyzing and Interpreting Air Monitoring Data. WHO Offset Publication No. 51, Geneva, Switzerland (Last Accessed January 24, 2017). http://apps.who.int/iris/bitstream/10665/37208/1/WHO_OFFSET_51.pdf.
Yienger, J.J., Galanter, M., Holloway, T.A., Phadnis, M.J., Guttikunda, S.K., Carmichael, G.R., Moxim, W.J., Levy II, H., 2000. The episodic nature of air pollution transport from Asia to North America. J. Geophys. Res. 106, 26931–26945.
Zhang, Y., Shotyk, W., Zaccone, C., Noernberg, T., Pellerier, R., Bicalho, B., Froese, D.G., Davies, L., Martin, J.W., 2016. Airborne petcoke dust is a major source of polycyclic aromatic hydrocarbons in the Athabasca Oil Sands Region. Environ. Sci. Technol. 50, 1711–1720.